Inorganic Chemistry

Article

pubs.acs.org/IC

Nitrate-to-Nitrite-to-Nitric Oxide Conversion Modulated by Nitrate-Containing $\{Fe(NO)_2\}^9$ Dinitrosyl Iron Complex (DNIC)

Fu-Te Tsai,*[,†] Yu-Ching Lee,[†] Ming-Hsi Chiang,[‡] and Wen-Feng Liaw*[,†]

[†]Department of Chemistry, National Tsing Hua University, Hsinchu 30013, Taiwan

[‡]Institute of Chemistry, Academic Sinica, NanKang, Taipei 115, Taiwan

Supporting Information

ABSTRACT: Nitrosylation of high-spin $[Fe(\kappa^2\text{-}O_2NO)_4]^{2-}$ (**1**) yields $\{Fe(NO)\}^7$ mononitrosyl iron complex (MNIC) $[(\kappa^2\text{-}O_2NO)(\kappa^1\text{-}ONO_2)_3Fe(NO)]^{2-}$ (**2**) displaying an $S = 3/2$ axial electron paramagnetic resonance (EPR) spectrum ($g_\perp = 3.988$ and $g_\parallel = 2.000$). The thermally unstable nitrate-containing $\{Fe(NO)_2\}^9$ dinitrosyl iron complex (DNIC) $[(\kappa^1\text{-}ONO_2)_2Fe(NO)_2]^-$ (**3**) was exclusively obtained from reaction of HNO_3 and $[(OAc)_2Fe(NO)_2]^-$ and was characterized by IR, UV−vis, EPR, superconducting quantum interference device (SQUID), X-ray absorption spectroscopy (XAS), and single-crystal X-ray diffraction (XRD). In contrast to $\{Fe(NO)_2\}^9$ DNIC $[(ONO)_2Fe(NO)_2]^-$ constructed by two monodentate O-bound nitrito ligands, the weak interaction between Fe(1) and the distal oxygens O(5)/O(7) of nitrato-coordinated ligands (Fe(1)···O(5) and Fe(1)···O(7) distances of 2.582(2) and 2.583(2) Å, respectively) may play important roles in stabilizing DNIC **3**. Transformation of nitrate-containing DNIC **3** into N-bound nitro $\{Fe(NO)\}^6$ $[(NO)(\kappa^1\text{-}NO_2)Fe(S_2CNEt_2)_2]$ (**7**) triggered by bis(diethylthiocarbamoyl) disulfide ($(S_2CNEt_2)_2$) implicates that nitrate-to-nitrite conversion may occur via the intramolecular association of the coordinated nitrate and the adjacent polarized NO-coordinate ligand (nitrosonium) of the proposed $\{Fe(NO)_2\}^7$ intermediate $[(NO)_2(\kappa^1\text{-}ONO_2)Fe(S_2CNEt_2)_2]$ (**A**) yielding $\{Fe(NO)\}^7$ $[(NO)Fe(S_2CNEt_2)_2]$ (**6**) along with the release of N_2O_4 ($\cdot NO_2$) and the subsequent binding of $\cdot NO_2$ to complex **6**. The N-bound nitro $\{Fe(NO)\}^6$ complex **7** undergoes Me_2S-promoted O-atom transfer facilitated by imidazole to give $\{Fe(NO)\}^7$ complex **6** accompanied by release of nitric oxide. This result demonstrates that nitrate-containing DNIC **3** acts as an active center to modulate nitrate-to-nitrite-to-nitric oxide conversion.

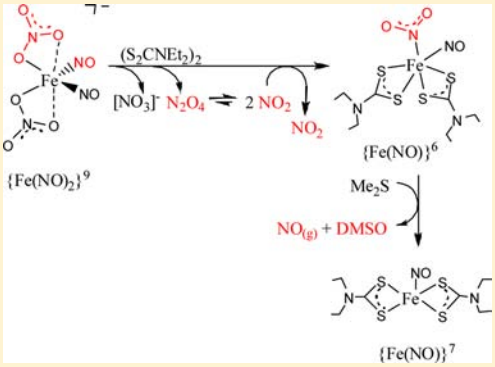

INTRODUCTION

Nitric oxide (NO) regulates a variety of physiological functions including vasodilation, neuron transmission, inflammation, immune response, and cancer therapy. Dinitrosyliron complexes (DNICs) are intrinsic NO-derived species that can serve as NO storage and transport in the biological systems.[1] In vivo, NO can be stabilized and stored in the form of protein-bound DNICs, and be probably released from cells in the form of low-molecular-weight DNIC (LMW-DNICs). Characterization of both protein-bound and low-molecular-weight DNICs in vitro has been made possible via their distinctive electron paramagnetic resonance (EPR) signal at $g = 2.03$.[2]

Nitrate ($[NO_3]^-$) and nitrite ($[NO_2]^-$) from endogenous or dietary sources are metabolized in vivo to generate nitric oxide.[3] The nitrate → nitrite → NO pathway is emerging as an important mediator of blood flow regulation, cell signaling, and energetic responses to hypoxia.[3] In comparison with substantially lower nitrite level (50−300 nM), normal plasma levels of nitrate are in the 20−40 μM range.[3a] Because human beings lack enzymes responsible for nitrate reduction yielding nitrite, the majority (60%) of nitrate is excreted in the urine unalternated. Nearly 25% of plasma nitrate stored in the salivary glands was converted into nitrite by bacteria nitrate reductase (molybdenum-containing enzyme).[3b]

In chemistry, syntheses and characterization of complexes $[Fe^{II}(\kappa^1\text{-}ONO_2)(TpivPP)]^-$ (TpivPP = *meso*-tetrakis(*o*-pivalamidophenyl) porphyrin), $[Fe^{III}(\kappa^2\text{-}O_2NO)(TPP)]$ (TPP = *meso*-tetraphenylporphyrin) and $[Fe^{III}(\kappa^1\text{-}ONO_2)(OEP)]$ (OEP = 2,3,7,8,12,13,17,18-octaethylporphyrin) were reported by Scheidt and co-workers.[4a,b] Ford and co-workers have shown that $Fe-O_{(NO3)}$ bond homolysis of $[(\kappa^1\text{-}ONO_2)Fe(NO)(TPP)]$ occurs via attack of exogenous NO at the oxygen of coordinated nitrate, leading to the formation of complex $[(TPP)Fe(NO)]$ accompanied by release of N_2O_4.[4c−f] In the nitrate reductase model study reported by Holm et al., complexes $[M^{IV}(QC_6H_2\text{-}2,4,6\text{-}{}^iPr_3)(S_2C_2Me_2)_2]^-$ (M = Mo, W; Q = S, O) promote O-atom transfer of the proposed coodinated nitrate to yield nitrite and $[M^{VI}(O)(QC_6H_2\text{-}2,4,6\text{-}{}^iPr_3)(S_2C_2Me_2)_2]^-$.[5a] In the catalytic cycle of nitrate activation triggered by molybdenum complex, the interconversion between $[Mo^{IV}(SPh)(mnt)_2]$ (mnt = 1,2-dicyanoethylenedithiolate) and $[Mo^{VI}(O)(SPh)(mnt)_2]$ along with the

Received: October 29, 2012
Published: December 13, 2012

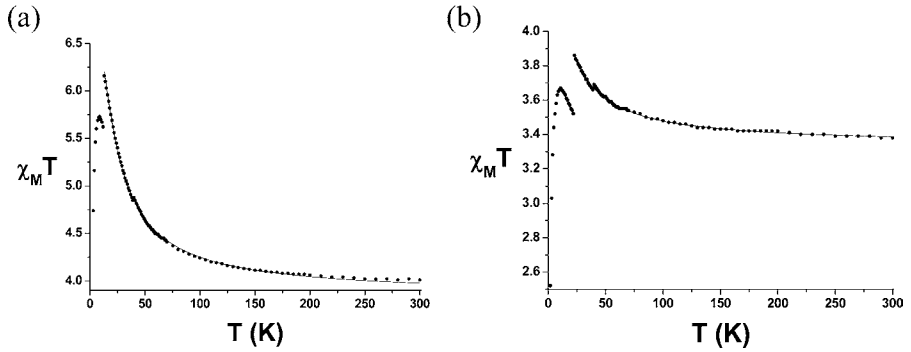

Figure 1. (a) Magnetic measurement of complex **1-PPN** under 1 T applied field. The best fit of $\chi_M T$ vs T plot gives $g = 2.262 \pm 0.001$, $|D| = 5.922 \pm 0.058$ cm^{-1}, $\theta = -1.156 \pm 0.046$ K ($R^2 = 0.999$). (b) Magnetic measurement of complex **1-Et$_4$N** under 1 T applied field. The best fit of $\chi_M T$ vs T plot gives $g = 2.110 \pm 0.001$, $|D| = 4.365 \pm 0.162$ cm^{-1}, $\theta = -4.489 \pm 0.272$ K ($R^2 = 0.997$).

generation of nitrite was demonstrated upon addition of nitrate into $[Mo^{IV}(SPh)(mnt)_2]$ and, reversibly, addition of PPh_3 into $[Mo^{VI}(O)(SPh)(mnt)_2]$ in CH_2Cl_2, respectively.[5b] To our best knowledge, no DNICs containing nitrato $[NO_3]^-$-coordinate ligands were described. Our previous study demonstrated that the distinct electronic structures of $\{Fe(NO)_2\}^{9/10}$ motifs ($\{Fe(NO)_2\}^9$ vs $\{Fe(NO)_2\}^{10}$) play crucial roles in modulating nitrite binding modes (O-bound chelating/monodentate nitrito for $\{Fe(NO)_2\}^9$ DNICs vs N-bound nitro as a π acceptor for $\{Fe(NO)_2\}^{10}$ DNICs), and in regulating nitrite activation pathways (O-atom abstraction by PPh_3 leading to the intermediate with nitroxyl coordinated ligand vs protonation accompanied by dehydration leading to the intermediate with nitrosonium coordinated ligand). That is, the redox shuttling between $\{Fe(NO)_2\}^9$ DNIC and $\{Fe(NO)_2\}^{10}$ DNIC modulates nitrite binding modes and then triggers nitrite activation to generate nitric oxide.[6] In this manuscript, synthesis of bidentate nitrato complex $[cation]_2[Fe(\kappa^2\text{-}O_2NO)_4]$ (**1**) (cation = PPN or Et_4N) and nitrosylation of complex **1** yielding mononitrosyl iron complex (MNIC) $[PPN]_2[(\kappa^2\text{-}O_2NO)(\kappa^1\text{-}ONO_2)_3Fe(NO)]$ (**2**) containing chelating and monodentate nitrato ligands were demonstrated. The unique synthetic route to the thermally unstable $\{Fe(NO)_2\}^9$ DNIC $[PPN][(\kappa^1\text{-}ONO_2)_2Fe(NO)_2]$ (**3**) containing nitrato-coordinated ligands was elucidated. The transformations $[PPN][(\kappa^1\text{-}ONO_2)(ONO)Fe(NO)_2]$ (**4**) ← **3** ⇌ $[PPN]_2[(\kappa^1\text{-}ONO_2)_2(\kappa^2\text{-}O_2NO)Fe(NO)_2]$ (**5**) were also discussed. Of importance, bis(diethylthiocarbamoyl) disulfide ($(S_2CNEt_2)_2$) triggering nitrate-to-nitrite-to-nitric oxide conversion mediated by nitrate-containing $\{Fe(NO)_2\}^9$ DNIC was uncovered.

RESULTS AND DISCUSSION

Nitrosylation of Chelating O-Bound Nitrato Complex $[Fe(\kappa^2\text{-}O_2NO)_4]^{2-}$ (1). Reaction of ferrous chloride, $AgNO_3$, and [cation][Cl] (cation = PPN, Et_4N) in a 1:4:2 molar ratio in MeCN at 0 °C yielded the thermally stable, light-yellow complex $[cation]_2[Fe(\kappa^2\text{-}O_2NO)_4]$ (**1**) (cation = PPN (**1-PPN**), yield 49%; cation = Et_4N (**1-Et$_4$N**), yield 45%) bearing four chelating O-bound nitrato ligands. Complex **1** was characterized by UV−vis spectroscopy and single-crystal X-ray diffraction (XRD). Compared to nitrite-containing complex $[PPN]_2[(ONO)_2Fe(\kappa^2\text{-}ONO)_2]$ exhibiting absorptions at 456 and 565 nm (CH_2Cl_2) at 233 K, the UV−vis spectrum of complex **1** in CH_2Cl_2 displays absorptions at 303, 327, and 380 nm at 273 K. The iron(II) center is in the high-spin electronic state. The magnetic susceptibility value of the powder sample of complex **1-PPN** increases from 1.34×10^{-2} cm^3 mol^{-1} (1.12×10^{-2} cm^3 mol^{-1} for **1-Et$_4$N**) at 300 K to 1.94 cm^3 mol^{-1} (1.26 cm^3 mol^{-1} for **1-Et$_4$N**) at 2 K. The corresponding $\chi_M T$ value of complex **1-PPN** increases from 4.01 cm^3 K mol^{-1} (3.38 cm^3 K mol^{-1} for **1-Et$_4$N**) at 300 K to 6.16 cm^3 K mol^{-1} (3.86 cm^3 K mol^{-1} for **1-Et$_4$N**) at 13 K (23 K for **1-Et$_4$N**), and then decreases to 3.87 cm^3 K mol^{-1} (2.52 cm^3 K mol^{-1} for **1-Et$_4$N**) at 2 K (Figure 1). It is noticed that the $\chi_M T$ and μ_{eff} values of complex **1-Et$_4$N** are smaller than those of complex **1-PPN**. Presumably, the smaller size of the cation (that is, Et_4N) in complex **1-Et$_4$N** induces the stronger intermolecular antiferromagnetic interactions ($\theta_{PPN} = -1.156$ K vs $\theta_{Et4N} = -4.489$ K) to lead to the smaller magnetic susceptibility, compared to that of complex **1-PPN**.

The lability of the nitrato ligands was demonstrated by the reaction of complex **1** with $[PPN][NO_2]$ in CH_2Cl_2. Treatment of CH_2Cl_2 solution of complex **1** with $[PPN][NO_2]$ in a 1:4 molar ratio at 0 °C led to the shift in the UV−vis spectrum from (303, 327, 380 nm) to (456, 565 nm), consistent with the formation of $[PPN]_2[(ONO)_2Fe(\kappa^2\text{-}ONO)_2]$ (Scheme 1a).[6b] Irreversibly, the addition of 4 equiv of $[PPN][NO_3]$ into $[(ONO)_2Fe(\kappa^2\text{-}ONO)_2]^{2-}$ in CH_2Cl_2 showing no spectroscopically detectable changes in UV−vis spectrum indicates that analogous nitrite displacement does not occur with this weaker base $[NO_3]^-$. This result demonstrates that the binding

Scheme 1

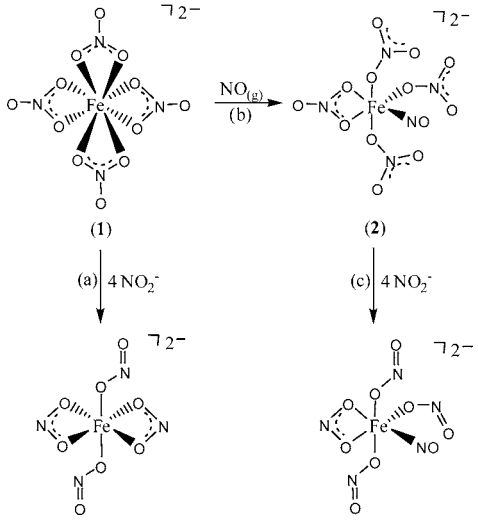

dx.doi.org/10.1021/ic3023437 | Inorg. Chem. 2013, 52, 464−473

preference of ligands $[NO_2]^-$ and $[NO_3]^-$ toward Fe(II) follows the ligand displacement series $[NO_2]^- > [NO_3]^-$. Presumably, the optimum electron-donating coordinated ligands tuning the optimum electronic structure of Fe(II) core affords the most stable complex $[(ONO)_2Fe(\kappa^2\text{-}ONO)_2]^{2-}$. These results may rationalize that the iron center of complex **1** is bound by four bidentate nitrato ligands, in contrast to the iron center of $[PPN]_2[(ONO)_2Fe(\kappa^2\text{-}ONO)_2]$ coordinated by two O-bound monodentate nitrito ligands and two O-bound bidentate nitrito ligands.

As shown in Scheme 1b, upon injection of NO gas (10% NO + 90% N_2) into a THF-MeCN (5: 1 mL) solution of complex **1-PPN** at 0 °C, a rapid reaction ensued over the course of 5 min to give the dark-red-brown $\{Fe(NO)\}^7$ mononitrosyl iron complex (MNIC) $[PPN]_2[(\kappa^2\text{-}O_2NO)(\kappa^1\text{-}ONO)_3Fe(NO)]$ (**2**) containing one bidentate nitrato ligand and three monodentate nitrato ligands, which was characterized by IR, EPR, UV−vis spectroscopy as well as single-crystal X-ray crystallography. In contrast to the phenylthiolate-ligand elimination yielding MNIC $[(PhS)_3Fe(NO)]^-$ observed in the nitrosylation of complex $[Fe(SPh)_4]^{2-}$,[7] NO radical binding to an electron-deficient ferrous center of complex **1-PPN** triggered nitrate linkage isomerization from bidentate to monodentate coordination to yield complex **2**. The higher NO stretching frequency of complex **2** (ν_{NO}: 1818 s cm^{-1} (CH_2Cl_2); 1830 s cm^{-1} (KBr)), compared to that of $[PPN]_2[(\kappa^2\text{-}ONO)(ONO)_3Fe(NO)]$ (IR(ν_{NO}): 1800 s cm^{-1} (CH_2Cl_2); 1768 s cm^{-1} (KBr)), may be attributed to the weaker electron-donating ability of nitrato ligands. At 4 K, complex **2** exhibits an $S = 3/2$ axial EPR spectrum with principal g values of $g_\perp = 3.988$ and $g_\parallel = 2.000$ (Figure 2),

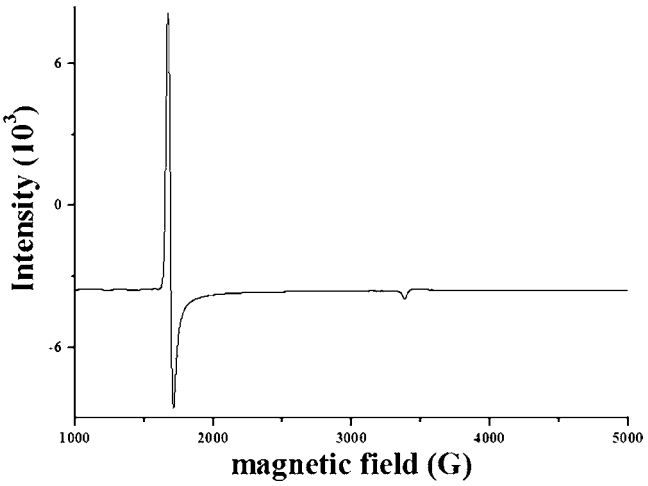

Figure 2. EPR spectrum of complex **2** at 4 K ($g_\perp = 3.988$ and $g_\parallel = 2.000$ (CH_2Cl_2)).

suggestive of the $\{Fe^{III}(NO^-)\}^7$ electronic structure.[7] The magnetic susceptibility value of the powder sample of complex **2** increases from 7.749×10^{-3} cm^3 mol^{-1} at 300 K to 0.637 cm^3 mol^{-1} at 2 K (Figure 3). The corresponding μ_{eff} value of 4.36 μ_B, compared to the spin-only value ($\mu_{eff} = 3.87$ μ_B) for $S = 3/2$ system, implicates that the magnetic ground state is the result of strong antiferromagnetic coupling between high spin Fe(III) ($S_{Fe} = 5/2$) and one nitroxyl ($S_{NO} = 1$).

To elucidate the stability and reactivity of complex **2** toward $[NO_2]^-$, reaction of complex **2** and $[NO_2]^-$ was investigated. Upon addition of 4 equiv of $[NO_2]^-$ into the CH_2Cl_2 solution

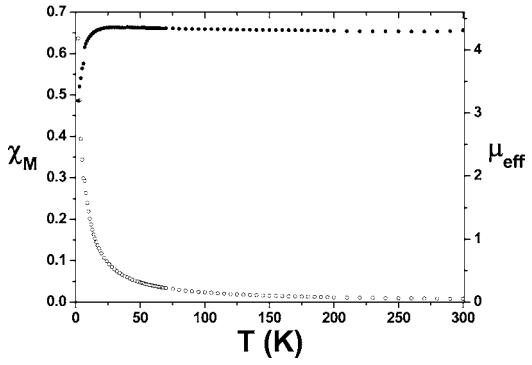

Figure 3. Magnetic measurement ((○) χ_M vs T; (●) μ_{eff} vs T) of the powder sample of complex **2** in a 1 T applied field.

of complex **2** at 0 °C, the IR ν_{NO} stretching frequency shifting from 1818 (s) cm^{-1} to 1800 (s) cm^{-1} implied the formation of $[PPN]_2[(\kappa^2\text{-}ONO)(ONO)_3Fe(NO)]$ (Scheme 1c).[6b] Presumably, the preferred formation of nitrite-containing $\{Fe(NO)\}^7$ MNIC $[(\kappa^2\text{-}ONO)(ONO)_3Fe(NO)]^{2-}$ via ligand-exchange reactions may be dictated by the thermodynamic preference for the stronger electron-donating ligands (as shown above, the electron-donating ability: $[NO_2]^- > [NO_3]^-$). In contrast to nitrosylation of MNIC $[(ON)Fe(SPh)_3]^-$ yielding DNIC $[(SPh)_2Fe(NO)_2]^-$ accompanied by reductive elimination of $(SPh)_2$,[7a] and PPh_3-triggered O-atom transfer of MNIC $[(\kappa^2\text{-}ONO)(ONO)_3Fe(NO)]^{2-}$ producing $OPPh_3$ as well as the known $\{Fe(NO)_2\}^9$ DNIC $[(ONO)_2Fe(NO)_2]^-$ via the proposed intermediate $[(ONO)_3Fe^{III}(NO)_2]^{2-}$,[6b] complex **2** is inert toward NO or PPh_3. That is, the chelating nitrato ligand of complex **2** does not undergo PPh_3-triggered O-atom transfer that may result in $[NO_3]^- \rightarrow [NO_2]^- \rightarrow [NO]^-$ transformation along with the production of the $\{Fe(NO)_2\}^9$ DNIC $[(\kappa^1\text{-}ONO_2)_2Fe(NO)_2]^-$. These results further support that redox-active ligands ($[SPh]^-$ for $[(ON)Fe(SPh)_3]^-$ and $[NO]^-$ derived from bidentate O-bound nitrito for $[(\kappa^2\text{-}ONO)(ONO)_3Fe(NO)]^{2-}$) are required for the transformation of $\{Fe(NO)\}^7$ MNICs into $\{Fe(NO)_2\}^9$ DNICs.[6b]

Synthesis of Nitrate-Containing DNIC $[PPN][(\kappa^1\text{-}ONO_2)_2Fe(NO)_2]$ (3). To synthesize nitrate-containing $\{Fe(NO)_2\}^9$ DNIC, reaction of $[(OAc)_2Fe(NO)_2]^-$ and HNO_3 was conducted. Addition of 2 equiv of aqueous nitric acid (16 M) into tetrahydrofuran (THF) solution of $\{Fe(NO)_2\}^9$ DNIC $[PPN][(OAc)_2Fe(NO)_2]$ at −10 °C yielded $\{Fe(NO)_2\}^9$ nitrate-containing DNIC $[PPN][(\kappa^1\text{-}ONO_2)_2Fe(NO)_2]$ (**3**) identified by IR, UV−vis, EPR spectroscopy, superconducting quantum interference device (SQUID), X-ray absorption spectroscopy (XAS), and single-crystal XRD (Scheme 2a). In contrast to the thermal stability of the nitrite-containing $\{Fe(NO)_2\}^9$ DNIC $[(ONO)_2Fe(NO)_2]^-$, complex **3** is thermally unstable in THF and solid state at room temperature. In comparison with the IR ν_{NO} stretching frequencies of $[(ONO)_2Fe(NO)_2]^-$ (1775 (s), 1705 (vs) cm^{-1} (THF)), complex **3** displaying the higher IR ν_{NO} stretching frequencies (1790 (s), 1710 (vs) cm^{-1} (THF)) is ascribed to the weaker electron-donating ability of the monodentate $[NO_3]^-$ ligands. The infrared spectrum of complex **3** shows strong bands at 1501 (sh), 1491 (s), 1283 (vs), and 806 (w) cm^{-1} (KBr) corresponding to the stretching frequencies of the bound nitrato groups. At 220 K, the EPR spectrum of complex **3** exhibits a well-resolved five-line hyperfine splitting signal with $g = 2.030$ ($A_N = 2.27$ G) (Figure 4a). With the aid of isotopic

dx.doi.org/10.1021/ic3023437 | Inorg. Chem. 2013, 52, 464−473

Scheme 2

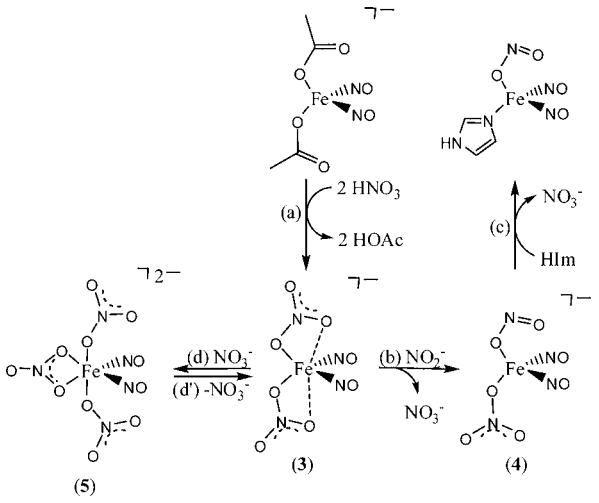

^{15}NO labeling experiments, the EPR spectrum of $[(\kappa^1\text{-}ONO_2)_2Fe(^{15}NO)_2]^-$ (**3-^{15}NO**) displaying a three-line hyperfine splitting signal at g = 2.031 (A^{15}_N = 3.45 G) rationalizes the unpaired electron coupling with nitrogens of two nitroxyl groups (Figure 4b). It is noticed that the ratio of hyperfine coupling constant of A^{14}_N and A^{15}_N is 0.66 in complex **3**.[9e] The magnetic susceptibility value of the powder sample of complex **3** increases from 1.957 × 10^{-3} cm^3 mol^{-1} at 300 K to 0.213 cm^3 mol^{-1} at 2 K (Supporting Information, Figure S1). The corresponding μ_{eff} value of 2.16 μ_B, compared to the spin-only value (μ_{eff} = 1.73 μ_B) for the S = 1/2 system, suggests that the magnetic ground state is the result of strong antiferromagnetic coupling between high spin Fe(III) (S_{Fe} = 5/2) and two nitroxyl ligands (S_{NO} = $S_{NO(1)}$ + $S_{NO(2)}$ = 2).[9] The reaction of $[PPN][NO_2]$ and complex **3** in 1:1 molar ratio in THF solution at −10 °C rapidly yielded $\{Fe(NO)_2\}^9$ nitrate-nitrite-containing DNIC $[PPN][(\kappa^1\text{-}ONO_2)(ONO)Fe(NO)_2]$ (**4**) (Scheme 2b).[9] The IR ν_{NO} stretching frequencies shifting from (1790 (s), 1710 (vs) cm^{-1}) to (1778 (s), 1707 (vs) cm^{-1}) suggested the formation of complex **4**. The IR absorption bands 1503 (sh), 1489 (s), 1286 (vs), and 807 (w) cm^{-1} (KBr) are assigned to the stretching frequencies of the bound nitrato ligand. At 298 K, complex **4** shows an isotropic EPR spectrum with signal at 2.032 (Supporting Information, Figure S2). Interestingly, when 1 equiv of imidazole (HIm) was added into the THF solution of complex **4**, the NO stretching frequencies shifting from (1778 (s), 1707 (vs) (cm^{-1})) to (1786 (s), 1716 (vs) (cm^{-1})) (THF) was assigned to the formation of the known complex $[(HIm)(ONO)Fe(NO)_2]$ (Scheme 2c).[6a] These results conclude that the binding preference for a given ligand ($[NO_2]^-$, HIm, $[NO_3]^-$) of the $\{Fe(NO)_2\}^9$ motif follows the ligand displacement series $[NO_2]^-$ > HIm > $[NO_3]^-$.

In contrast to the reaction of $[NO_2]^-$ and complex **3** yielding complex **4** via ligand-displacement reaction, addition of 1 equiv of $[PPN][NO_3]$ into the THF-MeCN solution of complex **3** led to the pseudo six-coordinate $\{Fe(NO)_2\}^9$ nitrato-containing DNIC $[PPN]_2[(\kappa^1\text{-}ONO_2)_2(\kappa^2\text{-}O_2NO)Fe(NO)_2]$ (**5**) characterized by IR, EPR spectroscopy, and single-crystal X-ray crystallography (Scheme 2d). Complex **5** displays the diagnostic IR ν_{NO} stretching frequencies 1750 (s), 1656 (vs) cm^{-1} (KBr). The structurally characterized complex **5** is stable only at temperatures lower than 200 K in CH_2Cl_2. At higher temperatures, complex **5** dissociates the weakly bidentate $[NO_3]^-$ ligand, and the initial complex **3** is completely restored at room temperature (Scheme 2d′). Presumably, the tendency of $[NO_3]^-$ chelation toward $[Fe(NO)_2]$ motif may play an important role in triggering dissociation of the bidentate $[NO_3]^-$ to convert complex **5** into complex **3** at room temperature, as observed in the single-crystal X-ray structure of complex **3** showing the weak interactions between Fe and the distal oxygens of the nitrato-coordinated ligands. The conversion of complex **3** to complex **5** upon adding 50 equiv of $[PPN][NO_3]$ into complex **3** in CH_2Cl_2 was observed by UV−vis spectroscopy at 183 K; the intense bands at 381, 513 nm disappeared, accompanied by the simultaneous formation of three absorption bands 375, 495, and 592 nm. Complex **5** exhibits a well-resolved five-line EPR signal with g_{av} = 2.031 and hyperfine coupling constant A_N = 2.24 G at 200 K (Figure 5). The magnetic susceptibility value of the powder sample of complex **5** increases from 2.018 × 10^{-3} cm^3 mol^{-1} at 300 K to 0.244 cm^3 mol^{-1} at 2 K (Supporting Information, Figure S3), and the corresponding μ_{eff} value is 2.22 μ_B.[9] The transformation of complex **3** into complex **5** under the presence of $[NO_3]^-$ further shows how the geometric structure and coordination number of $\{Fe(NO)_2\}^9$ DNICs were regulated by the electron-donating ability and conformation of the coordinated ligands $[NO_2]^-/[NO_3]^-$ (four-coordinate complex **3** vs four-coordinate complex **4** vs six-coordinate complex **5**). The stabilization of complex **5** promoted by the chelating $[NO_3]^-$-coordinated ligand implicates that the electron-deficient $[Fe(NO)_2]$ core of nitrato-containing DNIC **3** is tailored to minimize the electronic changes, modulated by associative coordination of

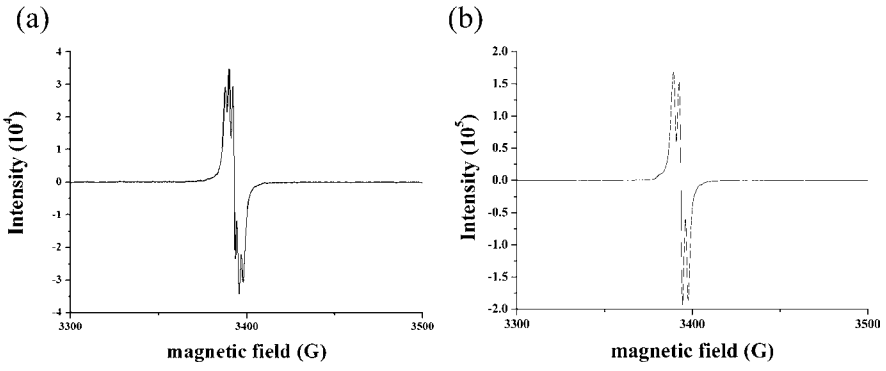

Figure 4. EPR spectra of (a) complex **3** in CH_2Cl_2 at 220 K (g_{av} = 2.030, A_N = 2.27 G), and (b) complex **3-^{15}NO** in CH_2Cl_2 at 220 K (g_{av} = 2.031, A^{15}_N = 3.45 G).

dx.doi.org/10.1021/ic3023437 | *Inorg. Chem.* 2013, 52, 464−473

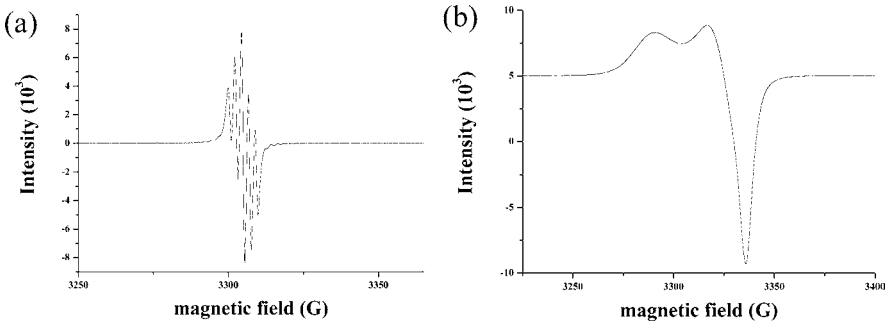

Figure 5. EPR spectra of complex **5** under the presence of 50-fold [PPN][NO_3] in CH_2Cl_2 at (a) 200 K (g_{av} = 2.031, A_N = 2.24 G), and (b) 77 K (g_1 = 2.044, g_2 = 2.022, g_3 = 2.017 and g_{av} = 2.028).

$[NO_3]^-$ yielding complex **5**, to preserve the $\{Fe(NO)_2\}^9$ electronic core of DNICs. It is presumed that the electron-donating ability is in the order of bidentate $[NO_3]^-$ > monodentate $[NO_3]^-$. Although the energy difference between the κ^1-NO_3 and κ^2-NO_3 isomers is small, as reported by density functional theory computations.[4c−f]

The Fe K-edge spectra of complexes **3** and **5** are shown in Figure 6. The Fe_{1s}→Fe_{3d} pre-edge transition is due to the d-p

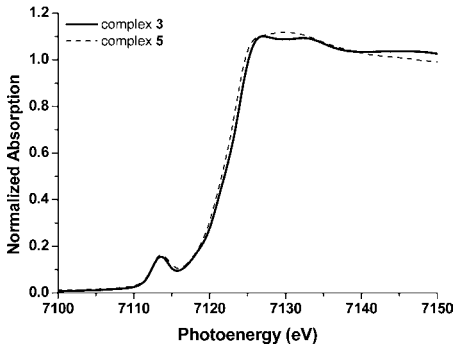

Figure 6. XAS Fe K-edge spectra of complexes **3** and **5**.

mixing between Fe and ligand atoms in the distorted T_d local environment of the Fe center.[9d] Compared to the tetrahedral $\{Fe(NO)_2\}^9$ DNIC $[(ONO)_2Fe(NO)_2]^-$ (7113.6 eV),[9d] complex **3** exhibiting identical pre-edge energy (7113.6 eV) may suggest that the effective nuclear charge (Z_{eff}) of Fe in complex **3** is similar to that of $[(ONO)_2Fe(NO)_2]^-$. It is noticed that the pre-edge energy (7113.7 eV) of complex **5** falls within the reported range of 7113.4−7113.8 eV for mononuclear $\{Fe(NO)_2\}^9$ DNICs.[9d]

Nitrate-to-Nitrite-to-Nitric Oxide Conversion Mediated by Nitrate-Containing $\{Fe(NO)_2\}^9$ DNIC. To uncover nitrate-to-nitrite conversion modulated by nitrate-containing $\{Fe(NO)_2\}^9$ DNIC, the reaction of complex **3** and bis(diethylthiocarbamoyl) disulfide ($(S_2CNEt_2)_2$) was conducted. As shown in Scheme 3, treatment of complex **3** with 1 equiv of $(S_2CNEt_2)_2$ in CH_2Cl_2 under N_2 atmosphere in the absence of light led to the formation of the known N-bound nitro $\{Fe(NO)\}^6$ $[(NO)(\kappa^1\text{-}NO_2)Fe(S_2CNEt_2)_2]$ (**7**) characterized by IR spectroscopy and single-crystal XRD (Supporting Information, Figure S6).[10a] The shift of IR ν_{NO} stretching frequencies from (1800, 1718 cm^{-1}) to 1847 cm^{-1} corroborated the formation of complex **7**. To elucidate the proposed mechanism, reaction of $[PPN][(\kappa^1\text{-}ONO_2)_2Fe(^{15}NO)_2]$ and $(S_2CNEt_2)_2$ was conducted. The appearance of 1847 cm^{-1} (ν^{14}_{NO}) and 1815 cm^{-1} (ν^{15}_{NO}) stretching frequencies

Scheme 3

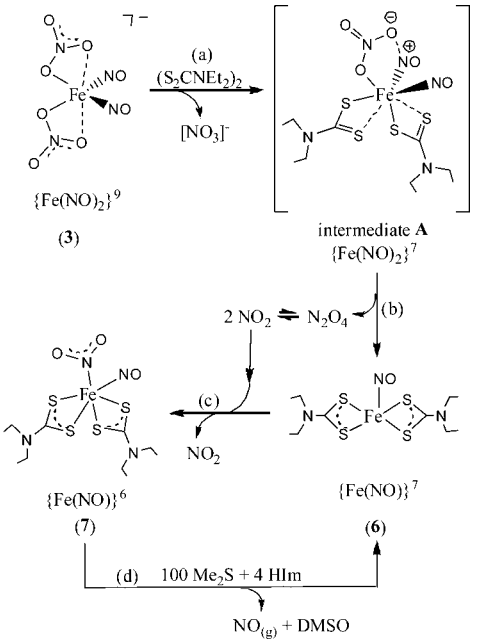

corroborated isotopic scrambling between $[^{14}NO_2]^-$ and ^{15}NO.[10b] The reaction sequences (nitrate-to-nitrite conversion) given in Scheme 3 may reasonably account for the transformation of complex **3** into complex **7**: Oxidative addition of $(S_2CNEt_2)_2$ to $\{Fe(NO)_2\}^9$ complex **3** generates the proposed $\{Fe(NO)_2\}^7$ intermediate **A** (Scheme 3a). The subsequent chelation of $[S_2CNEt_2]^-$ ligands to iron followed by intramolecular association of nitrate and nitrosonium (the NO-coordinate ligand of $\{Fe(NO)_2\}^7$ intermediate **A** being polarized from the approach of the adjacent coordinated nitrate) triggers the formation of $\{Fe(NO)\}^7$ $[(NO)Fe(S_2CNEt_2)_2]$ (**6**) accompanied by the release of $N_2O_{4(g)}$ (Scheme 3b).[9b,c] Subsequently, nitrogen dioxide ($\cdot NO_2$) derived from thermal equilibrium of N_2O_4 oxidizes $\{Fe(NO)\}^7$ complex **6** to yield N-bound nitro $\{Fe(NO)\}^6$ complex **7** (Scheme 3c).[10a] To trap the produced redundant nitrogen dioxide ($\cdot NO_2$), reaction of complex **3**, $(S_2CNEt_2)_2$ and $\{Fe(NO)\}^7$ $[(NO)Fe(S_2CNEt_2)_2]$ (1:1:0.3 molar ratio) in CH_2Cl_2 was conducted. The complete shift of IR ν_{NO} stretching frequencies from 1800, 1718, 1712 cm^{-1} (mixture of complex **3** and $[(NO)Fe(S_2CNEt_2)_2]$) to 1847 cm^{-1} (complex **7**) indicated that 65% of produced $\cdot NO_2$ was trapped.

The nitrite-to-nitric oxide conversion was observed when THF solution of the N-bound nitro $\{Fe(NO)\}^6$ complex **7** was

dx.doi.org/10.1021/ic3023437 | Inorg. Chem. 2013, 52, 464−473

treated with 100-fold of dimethyl sulfide (Me_2S) under the presence of 4 equiv of imidazole (HIm) in the absence of light at room temperature (Scheme 3d).[11] The IR ν_{NO} stretching frequency shifting from 1835 cm^{-1} to 1716 cm^{-1} (THF) indicated the transformation of $\{Fe(NO)\}^6$ complex **7** into $\{Fe(NO)\}^7$ complex **6**. The sequences of reaction may be rationalized as follows: Hydrogen-binding interaction between HIm and N-bound nitro of $\{Fe(NO)\}^6$ complex **7** facilitates dimethyl sulfide to trigger oxygen-atom transfer of N-bound nitro to yield the proposed thermally unstable $\{Fe(NO)_2\}^8$ intermediate $[(NO)_2Fe(S_2CNEt_2)_2]$. The followed elimination of $NO_{(g)}$ generates $\{Fe(NO)\}^7$ complex **6**. The released nitric oxide was trapped by $[PPN]_2[S_5Fe(\mu\text{-}S)_2FeS_5]$ to produce the known $[PPN][S_5Fe(NO)_2]$ (70%).[9g] The produced dimethyl sulfoxide (DMSO) was characterized by ^1H NMR (δ = 2.56 ppm (C_4D_8O)) (Supporting Information, Figure S4). This result demonstrates that nitrate-containing $\{Fe(NO)_2\}^9$ DNIC may serve as an intermediary for the conservation of NO, and act as an active center to regulate the transformation of nitrate into nitrite and then nitric oxide.

Structures. The single-crystal X-ray structures of complexes **1-PPN** and **2** are displayed in Figures 7 and 8, and selected

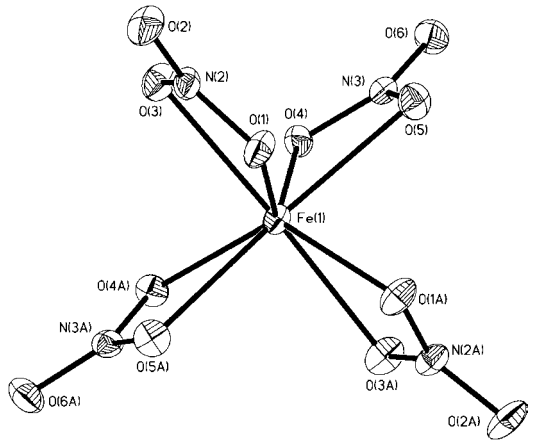

Figure 7. ORTEP drawing and labeling scheme of complex **1** with thermal ellipsoids drawn at 30% probability. Selected bond lengths (Å) and angles (deg): Fe(1)−O(1) 2.182(1), Fe(1)−O(3) 2.321(1), Fe(1)−O(4) 2.194(1), Fe(1)−O(5) 2.317(1); O(1)−Fe(1)−O(3) 56.9(1), O(5)−Fe(1)−O(4) 56.9(0). Two PPN^+ cations are omitted for clarity.

bond distances and angles are presented in the figure captions, respectively. The most striking feature of complex **1-PPN** is that the iron is located at the center of the O_8 environment composed of four bidentate nitrato ligands with Fe(1)−O(1), Fe(1)−O(3), Fe(1)−O(4), Fe(1)−O(5) bond lengths of 2.182(1), 2.321(1), 2.194(1), 2.317(1) Å, respectively. The O(1)−Fe(1)−O(4), O(1)−Fe(1)−O(5), O(1)−Fe(1)−O(3), O(4)−Fe(1)−O(3), O(4)−Fe(1)−O(5), and O(3)−Fe(1)−O(5) bond angles of 129.5(1)°, 89.3(1)°, 56.9(1)°, 85.6(1)°, 56.9(1)°, and 92.2(1)°, respectively, are consistent with the distorted pseudo eight-coordinate environment about the iron site of complex **1-PPN**.

The single-crystal X-ray structure of complex **2** is found to have the orthorhombic $P2_12_12_1$ space group. The iron center in complex **2** adopts an octahedral geometry consisting of one NO molecule, one bidentate nitrato ligand, and three monodentate nitrato ligands. The constraint of the bidentate nitrato generates a O(1)−Fe(1)−O(2) bond angle of 58.9(1)°

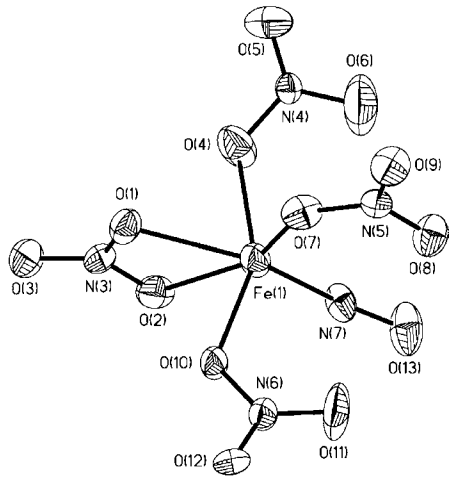

Figure 8. ORTEP drawing and labeling scheme of complex **2** with thermal ellipsoids drawn at 30% probability. Selected bond lengths (Å) and angles (deg): Fe(1)−N(7) 1.779(7), Fe(1)−O(1) 2.222(3), Fe(1)−O(2) 2.155(3), Fe(1)−O(4) 2.096(3), Fe(1)−O(7) 1.903(9), Fe(1)−O(10) 2.094(3), N(7)−O(13) 1.177(8); Fe(1)−N(7)−O(13) 164.1(7), O(1)−Fe(1)−O(2) 58.9(1). Two PPN^+ cations are omitted for clarity. The partition ratio 68.5: 31.5 is used to model substitutional disorder between NO and monodentate nitrato ligand.

enforcing a severe distortion at the six-coordinate iron site. The N(7)−O(13) bond length of 1.177(8) Å falls in the reported range of $\{Fe(NO)\}^7$ mononitrosyliron complexes (MNICs), ranging from 1.002(9) to 1.193(4) Å. Also, the Fe(1)−N(7) bond length of 1.779(7) Å in complex **2** is near the upper end of the reported Fe−N(O) bond lengths, ranging from 1.659(6) to 1.779(9) Å, of the $\{Fe(NO)\}^7$ MNICs.[7]

Figures 9, 10, and Supporting Information, Figure S5 display the thermal ellipsoid plots of complexes **3**, **4**, and **5**, respectively, and the selected bond lengths and bond angles were presented in figure captions. The geometry of iron center of complex **3** is a distorted tetrahedron with N(2)−Fe(1)−

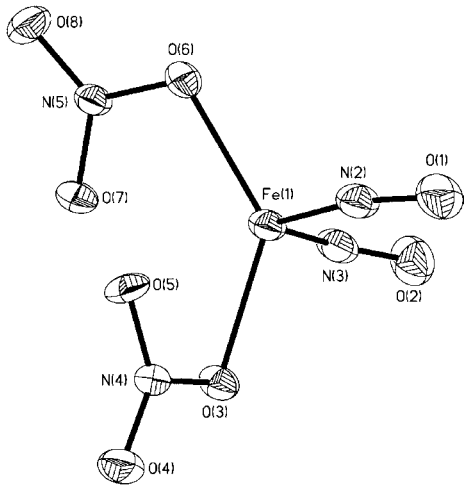

Figure 9. ORTEP drawing and labeling scheme of complex **3** with thermal ellipsoids drawn at 30% probability. Selected bond lengths (Å) and angles (deg): Fe(1)−N(2) 1.701(3), Fe(1)−N(3) 1.704(3), N(2)−O(1) 1.172(4), N(3)−O(2) 1.178(4), Fe(1)−O(3) 2.029(2), Fe(1)−O(6) 2.049(2); Fe(1)−N(2)−O(1) 161.3(3), Fe(1)−N(3)−O(2) 159.4(3), N(2)−Fe(1)−N(3) 109.7(2), O(3)−Fe(1)−O(6) 132.9(1). PPN^+ cation is omitted for clarity.

dx.doi.org/10.1021/ic3023437 | Inorg. Chem. 2013, 52, 464−473

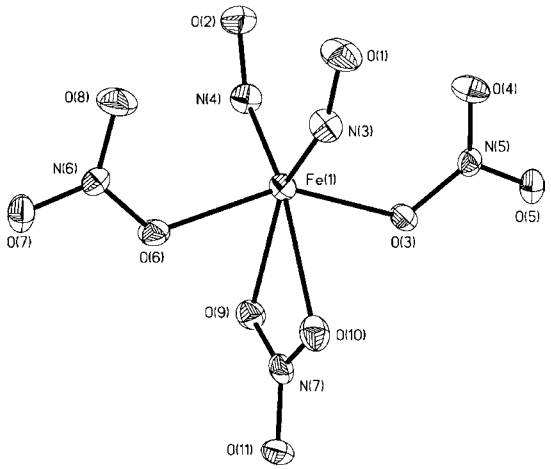

Figure 10. ORTEP drawing and labeling scheme of complex **5** with thermal ellipsoids drawn at 30% probability. Selected bond lengths (Å) and angles (deg): Fe(1)−N(3) 1.723(4), Fe(1)−N(4) 1.730(4), Fe(1)−O(3) 2.133(3), Fe(1)−O(6) 2.142(3), Fe(1)−O(9) 2.232(3), Fe(1)−O(10) 2.350(3), N(3)−O(1) 1.172(5), N(4)−O(2) 1.170(5); Fe(1)−N(3)−O(1) 148.3(4), Fe(1)−N(4)−O(2) 148.4(3), O(9)−Fe(1)−O(10) 56.4(1), N(3)−Fe(1)−N(4) 99.5(2), O(3)−Fe(1)−O(6) 148.0(1). Two PPN^+ cations are omitted for clarity.

N(3), N(2)−Fe(1)−O(3), N(2)−Fe(1)−O(6), and N(3)−Fe(1)−O(6) bond angles of 109.7(2)°, 103.6(1)°, 102.7(1)°, and 109.0(1)°, respectively. It is noticed that the Fe(1)···O(5) and Fe(1)···O(7) distances of 2.582(2) and 2.583(2) Å indicates the weak interaction between the Fe center and the distal oxygens of the coordinated nitrato ligands. Presumably, the presence of Fe(1)···O(5) and Fe(1)···O(7) interactions play crucial roles in stabilizing DNIC **3**. The N−O bond lengths of 1.172(4) and 1.178(4) Å in complex **3** are within the published N−O bond lengths, ranging from 1.160(6) to 1.186(7) Å, of the $\{Fe(NO)_2\}^9$ DNICs.[6−9] It is noticed that the Fe(1)−N(O) bond lengths of 1.701 (3) and 1.704(3) Å in complex **3** are close to those of the reported $\{Fe(NO)_2\}^9$ DNICs ranging from 1.661(4) to 1.695(3) Å.[6−9] The iron center of complex **4** exhibits the distorted tetrahedral geometry with N(2)−Fe(1)−N(3), N(2)−Fe(1)−O(3), N(3)−Fe(1)−O(3), and N(3)−Fe(1)−O(5) bond angles of 110.2(1)°, 108.3(1)°, 101.7(1)°, and 103.4(1)°, respectively. The longer Fe(1)···O(4) distance of 2.616(3) Å in complex **4**, as compared with the Fe(1)···O(5) and Fe(1)···O(7) distances of 2.582(2) and 2.583(2) Å in complex **3**, is attributed to the stronger electron donation of the coordinated nitrito ligand which stabilizes the $\{Fe(NO)_2\}^9$ DNIC **4**. The Fe(1)−N(2) and Fe(1)−N(3) bond lengths of 1.703(3) and 1.704(3) Å are comparable to the published Fe−N bond lengths, ranging from 1.661(4) to 1.695(3) Å, of the anionic $\{Fe(NO)_2\}^9$ DNICs. Also, the N(2)−O(1) and N(3)−O(2) bond lengths of 1.174(4) and 1.174(4) Å is within the range 1.160(6)−1.178(3) Å observed for the anionic $\{Fe(NO)_2\}^9$ DNICs.[6−9]

The iron of complex **5** is located at the center of N_2O_4 environment composed of two monodentate nitrato ligands, one bidentate nitrato ligand, and two NO ligands. The O(3)−Fe(1)−O(6) bond angle of complex **5** is 148.0(1)°. The constraint of the bidentate nitrato generates a O(9)−Fe(1)−O(10) bond angle of 56.4(1)° enforcing a severe distortion from an octahedron at the six-coordinate iron site. Surprisingly, the Fe(1)−N(3) and Fe(1)−N(4) bond lengths of 1.723(4) and 1.730(4) Å in complex **5**, significantly longer than those of the reported Fe−N(O) bond lengths (ranging from 1.661(4) to 1.695(3) Å) of the four-coordinate $\{Fe(NO)_2\}^9$ DNICs, probably originate from the steric effect between two coordinated NO ligands. Compared to the average Fe−N−O bond angles of 150.1(3)° (149.3(3) and 151.0(3)°) observed in complex $[(1\text{-MeIm})_2(\kappa^2\text{-ONO})Fe(NO)_2]$ (1-MeIm = 1-methylimidazole),[6a] the Fe(1)−N(3)−O(1) and Fe(1)−N(4)−O(2) bond angles of 148.3(4)° and 148.4(3)° are smaller than those of the published four-coordinate DNICs ranging from 157.1(2)° to 172.1(3)°.[6−9]

CONCLUSION AND COMMENTS

Study on the nitrate-containing $\{Fe(NO)\}^7$ MNIC and $\{Fe(NO)_2\}^9$ DNICs have led to the following results.

(1) The nitrate-containing $\{Fe(NO)_2\}^9$ DNIC **3** was exclusively obtained from addition of 2 equiv of aqueous nitric acid into THF solution of $\{Fe(NO)_2\}^9$ DNIC $[(OAc)_2Fe(NO)_2]^-$ at −10 °C. In contrast to the thermally stable, tetrahedral nitrito-coordinate DNIC $[(\kappa^1\text{-ONO})_2Fe(NO)_2]^-$, the isolated $\{Fe(NO)_2\}^9$ DNIC **3** characterized by single-crystal XRD is, presumably, stabilized with the presence of the weak interaction between the Fe center and the distal oxygens of the coordinated nitrato ligands (Fe(1)···O(5) and Fe(1)···O(7) distances of 2.582(2) and 2.583(2) Å, respectively).

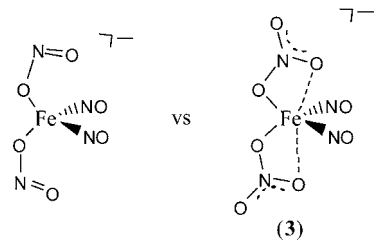

(2) In combination with XAS Fe K-edge pre-edge energy (7113.6 eV) and EPR spectrum of complex **3** displaying a five-line hyperfine splitting signal with g = 2.030 (A_N = 2.27 G) at 220 K, EPR spectrum of isotopic labeling **3-^{15}NO** showing a three-line signal at g = 2.031 (A^{15}_N = 3.45 G) with A^{14}_N/A^{15}_N = 0.66 implicates that the antiferromagnetic coupling occurs between high spin Fe(III) (S_{Fe} = 5/2) and two nitroxyl ligands ($S_{NO} = S_{NO(1)} + S_{NO(2)} = 2$).

(3) Irreversibly, quantitative transformation of the nitrate-containing $\{Fe(NO)\}^7$ MNIC **2** to nitrite-containing MNIC $[(\kappa^2\text{-ONO})(ONO)_3Fe(NO)]^{2-}$ was demonstrated. The corresponding μ_{eff} value of 4.36 μ_B and EPR spectrum of complex **2** exhibiting an S = 3/2 axial spectrum with principal g value of $g_\perp$ = 3.988 and $g_\parallel$ = 2.000 suggest that the electronic structure of $\{Fe(NO)\}$ core of MNIC **2** is best described as $\{Fe^{III}(NO^-)\}^7$.

(4) The binding preference for a given ligand ($[NO_2]^-$, HIm, $[NO_3]^-$) of the $\{Fe(NO)_2\}^9$ motif follows the ligand displacement series $[NO_2]^-$ > HIm > $[NO_3]^-$.

(5) In contrast to the inertness of $\{Fe(NO)_2\}^9$ DNIC $[(ONO)_2Fe(NO)_2]^-$ toward $[NO_3]^-$, the stabilization of nitrate-containing DNICs **5** and **4** implicates that the electron-deficient $[Fe(NO)_2]$ core of DNIC **3** is tailored to minimize the electronic changes, regulated by associative coordination of $[NO_3]^-$ yielding complex **5** and ligand displacement yielding complex **4**, to preserve the $\{Fe(NO)_2\}^9$ electronic core.

(6a) **Nitrate-to-nitrite conversion triggered by bis(diethylthiocarbamoyl) disulfide ($(S_2CNEt_2)_2$).** Transforma-

dx.doi.org/10.1021/ic3023437 | Inorg. Chem. 2013, 52, 464−473

tion of nitrate-containing DNIC **3** into N-bound nitro $\{Fe(NO)\}^6$ **7** triggered by $(S_2CNEt_2)_2$ suggests that intramolecular association of the coordinated nitrate and the adjacent polarized NO-coordinate ligand (nitrosonium) of $\{Fe(NO)_2\}^7$ intermediate $[(NO)_2(\kappa^1\text{-}ONO_2)Fe(S_2CNEt_2)_2]$ (**A**) leads to the formation of $\{Fe(NO)\}^7$ **6** along with the release of N_2O_4 ($\cdot NO_2$). Nitrogen dioxide ($\cdot NO_2$) derived from thermal equilibrium of N_2O_4 oxidizes $\{Fe(NO)\}^7$ **6** to generate N-bound nitro $\{Fe(NO)\}^6$ **7**.

(6b) **Nitrite-to-nitric oxide conversion promoted by dimethyl sulfide (Me_2S).** The N-bound nitro of $\{Fe(NO)\}^6$ **7** undergoes Me_2S-promoted oxygen-atom transfer facilitated by imidazole to produce the proposed thermally unstable $\{Fe(NO)_2\}^8$ intermediate $[(NO)_2Fe(S_2CNEt_2)_2]$. The followed $NO_{(g)}$ elimination generates $\{Fe(NO)\}^7$ **6**. This result demonstrates that nitrate-containing $\{Fe(NO)_2\}^9$ DNIC **3** acts as an active center to modulate nitrate-to-nitrite-to-nitric oxide conversion.

These results may lend credence to the proposal that nitrate-containing $\{Fe(NO)_2\}^9$ DNICs **3**, **4**, and **5** serve as endogenous $NO/[NO_3]^-$ storage and transport in the biological systems, and nitrate-to-nitrite-to-nitric oxide conversion is mediated by nitrate-containing $\{Fe(NO)_2\}^9$ DNIC in biological conditions.

EXPERIMENTAL SECTION

Manipulations, reactions, and transfers were conducted under N_2 according to Schlenk techniques or in a glovebox (N_2 gas). Solvents were distilled under N_2 from appropriate drying agents (acetonitrile from CaH_2–P_2O_5; diethyl ether, hexane, and THF from sodium benzophenone) and stored in dried, N_2-filled flasks over 4 Å molecular sieves. N_2 was purged through these solvents before use. The solvent was transferred to the reaction vessel via a stainless cannula under positive pressure of N_2. Dimethyl sulfide (Me_2S) was stored over sodium in a gastight flask to remove trace quantity of thiol and water and distilled before using.[11] The reagents aqueous nitric acid (16 M), silver nitrate, and bis(triphenylphosphoranylidene)ammonium chloride ([PPN][Cl]) were used as received. Compound $[PPN][(NO)_2Fe(OAc)_2]$ was synthesized by published procedures.[6b] Infrared spectra of the ν(NO) and $\nu(NO_3)$ stretching frequencies were recorded on a Perkin-Elmer model spectrum one B spectrophotometer with sealed solution cells (0.1 mm, CaF_2 windows) or KBr disc. UV–vis spectra were recorded on a Jasco V-570. ^{1}H NMR spectrum was obtained on a Varian Unity-500 spectrometer. Analyses of carbon, hydrogen, and nitrogen were obtained with a CHN analyzer (Heraeus).

Preparation of $[PPN]_2[Fe(\kappa^2\text{-}O_2NO)_4]$ (1-PPN). $FeCl_2$ (0.13 g, 1 mmol), [PPN][Cl] (1.15 g, 2 mmol), and $AgNO_3$ (0.77 g, 4 mmol) were dissolved in MeCN (5 mL) under N_2 atmosphere. The mixture solution was stirred for 1 h at 0 °C. The resulting yellow solution was filtered through Celite to remove the insoluble solid (presumably, AgCl). Diethyl ether was then added slowly to layer above the filtrate. The flask was tightly sealed and kept in the refrigerator at −20 °C for 2 weeks to yield yellow crystals $[PPN]_2[Fe(\kappa^2\text{-}O_2NO)_4]$ (**1**) (yield 0.34 g, 49%) suitable for XRD analysis. Absorption spectrum (CH_2Cl_2) [λ_{max}, nm (ε, M^{-1} cm^{-1})]: 262 (8305), 267 (8676), 275 (6982), 303 (1250), 327 (898), 380 (265). Anal. Calcd. for $C_{72}H_{60}P_4FeN_6O_{12}$: C, 62.62; H, 4.38; N, 6.09. Found: C, 61.95; H, 4.40; N, 6.07.

Reaction of Complex 1-PPN with 4 equiv of $[PPN][NO_2]$. A MeCN solution of complex **1-PPN** (0.1382 g, 0.1 mmol) was transferred into a Schlenk tube containing $[PPN][NO_2]$ (0.24 g, 0.4 mmol) under the positive N_2 pressure at 0 °C. After the reaction was stirred for 40 min, the shift in UV–vis spectrum from (303, 327, 380 nm) to (456, 565 nm) was assigned to the formation of $[PPN]_2[(ONO)_2Fe(\kappa^2\text{-}ONO)_2]$.[6b] Diethyl ether was then added slowly to layer above the solution. The flask was tightly sealed and kept in the refrigerator at −20 °C for 2 weeks to yield white crystals $[PPN][NO_3]$ and the known red-brown crystals $[PPN]_2[(ONO)_2Fe(\kappa^2\text{-}ONO)_2]$.[6b]

Preparation of $[PPN]_2[(\kappa^2\text{-}O_2NO)(\kappa^1\text{-}O_2NO)_3Fe(NO)]$ (2). NO gas (24 mL, 10% NO + 90% N_2) was injected into the THF-MeCN solution (3 mL) of complex **1** (0.69 g, 0.5 mmol) by gastight syringe at 0 °C. After the reaction solution was stirred for 30 min at 0 °C, the dark red-brown solution was filtered through Celite to remove the insoluble solid. Diethyl ether was then added slowly to layer above the filtrate. The flask was tightly sealed and kept in the refrigerator at −20 °C for 2 weeks to yield red-brown crystals $[PPN]_2[(\kappa^2\text{-}O_2NO)(\kappa^1\text{-}O_2NO)_3Fe(NO)]$ (**2**) (yield 0.18 g, 26%) suitable for XRD analysis. IR (cm^{-1}): 1818 (ν_{NO}) (CH_2Cl_2). Absorption spectrum (CH_2Cl_2) [λ_{max}, nm (ε, M^{-1} cm^{-1})]: 244 (1104), 261 (845), 268 (884), 374 (672), 450 (310), 578 (158). Anal. Calcd. for $C_{72}H_{60}P_4FeN_7O_{13}$: C, 61.29; H, 4.29; N, 6.95. Found: C, 60.50; H, 4.22; N, 6.66.

Reaction of Complex 2 with 4 equiv of $[PPN][NO_2]$. To a flask containing $[PPN][NO_2]$ (0.24 g, 0.4 mmol) was added the CH_2Cl_2 solution of complex **2** (0.141 g, 0.1 mmol) at 0 °C. After the reaction was stirred for 20 min, The IR ν_{NO} stretching frequencies shifting from 1818 (s) cm^{-1} to 1800 (s) cm^{-1} was assigned to the formation of $[PPN]_2[(\kappa^2\text{-}ONO)(ONO)_3Fe(NO)]$.[6b] Diethyl ether was then added slowly to layer above the solution. The flask was tightly sealed and kept in the refrigerator at −20 °C for 2 weeks to yield white crystals $[PPN][NO_3]$ and the known red-brown crystals $[PPN]_2[(\kappa^2\text{-}ONO)(ONO)_3Fe(NO)]$.[6b]

Preparation of $[PPN][(\kappa^1\text{-}ONO_2)_2Fe(NO)_2]$ (3). To a THF solution of complex $[PPN][(NO)_2Fe(OAc)_2]$ (0.773 g, 1.0 mmol) was added 0.13 mL of $HNO_{3(aq)}$ (16 M, 2.0 mmol) by gastight syringe under N_2 atmosphere at −10 °C. After stirring for 5 min, a large amount of cold hexane (−10 °C) was added to precipitate the dark semi-oily complex $[PPN][(\kappa^1\text{-}ONO_2)_2Fe(NO)_2]$ (**3**) (yield 0.61 g, 78%). Crystals suitable for XRD analysis were obtained from the THF solution of complex **3** layered with hexane at −20 °C for 2 weeks. IR (cm^{-1}): 1790 (s), 1710 (vs) (ν_{NO}), 1494 (ν_{NO3}) (THF); 1800 (s), 1718 (vs) (ν_{NO}), 1493 (ν_{NO3}) (CH_2Cl_2); 1790 (s), 1710 (vs) (ν_{NO}), 1501, 1491, 1283, 806 (ν_{NO3}) (KBr). $[PPN][(\eta^1\text{-}O^{15}NO_2)_2Fe(NO)_2]$ (**3-$^{15}NO_3$**) IR (cm^{-1}): 1800 (s), 1718 (vs) (ν_{NO}), 1456 (ν_{15NO3}) (CH_2Cl_2); 1790 (s), 1710 (vs) (ν_{NO}), 1464, 1456, 1252, 786 (ν_{15NO3}) (KBr). Absorption spectrum (CH_2Cl_2) [λ_{max}, nm (ε, M^{-1} cm^{-1})]: 381 (931), 513 (334). Anal. Calcd. for $C_{36}H_{30}P_2FeN_5O_8$: C, 55.49; H, 3.85; N, 9.00. Found: C, 55.62; H, 4.03; N, 8.79.

Preparation of $[PPN][(ONO)(\kappa^1\text{-}ONO_2)Fe(NO)_2]$ (4). To a 30-mL Schlenk tube loaded with complex **3** (0.778 g, 1.0 mmol) was added the CH_2Cl_2 solution of $[PPN][NO_2]$ (0.585 g, 1.0 mmol) at −10 °C. After stirring for 10 min, cold hexane (−10 °C) was added to lead to the precipitation of the dark solid $[PPN][(ONO)(\kappa^1\text{-}ONO_2)Fe(NO)_2]$ (yield 0.64 g, 82%). Crystals suitable for XRD analysis were obtained from the THF solution of complex **4** layered with hexane at −20 °C for 2 weeks. IR (cm^{-1}): 1778 (s), 1707 (vs) (ν_{NO}), 1494 (ν_{NO3}) (THF); 1789 (s), 1715 (vs) (ν_{NO}), 1494 (ν_{NO3}) (CH_2Cl_2); 1783 (s), 1711 (vs) (ν_{NO}), 1503, 1489, 1286, 807 (ν_{NO3}) (KBr). $[PPN][(ONO)(\eta^1\text{-}O^{15}NO_2)Fe(NO)_2]$ (**4-$^{15}NO_3$**) IR (cm^{-1}): 1789 (s), 1715 (vs) (ν_{NO}), 1453 (ν_{15NO3}) (CH_2Cl_2); 1783 s, 1711 vs (ν_{NO}), 1468, 1453, 1260, 787 (ν_{15NO3}) (KBr). Absorption spectrum (CH_2Cl_2) [λ_{max}, nm (ε, M^{-1} cm^{-1})]: 382 (923), 510 (348). Anal. Calcd. for $C_{36}H_{30}P_2FeN_5O_7$: C, 56.65; H, 3.93; N, 9.18. Found: C, 57.05; H, 4.27; N, 9.03.

Reaction of Complex 4 with 1 equiv of HIm (HIm = imidazole). To a 30-mL Schlenk tube loaded with complex **4** (0.762 g, 1.0 mmol) was added the THF solution (3 mL) of HIm (0.07 g, 1.0 mmol) at −10 °C. After stirring for 30 min, the NO stretching frequencies shifting from (1778 (s), 1707 (vs) cm^{-1}) to (1786 (s), 1716 (vs) cm^{-1}) (THF) was assigned to the formation of the known complex $[(HIm)(ONO)Fe(NO)_2]$.[6a] Diethyl ether (4 mL) was added into the resulting solution to precipitate $[PPN][NO_3]$. The resulting mixture was filtered through Celite to remove the insoluble solid. A large amount of hexane (80 mL) was added to lead to the precipitation of the known dark solid $[(HIm)(ONO)Fe(NO)_2]$ (yield 0.17 g, 73%).[6a]

Preparation of $[PPN]_2[(\kappa^2\text{-}O_2NO)(\kappa^1\text{-}ONO_2)_2Fe(NO)_2]$ (5). Complex **3** (0.15 g, 0.2 mol) and $[PPN][NO_3]$ (0.11 g, 0.2 mmol) were loaded into a Schlenk tube and dissolved in THF-MeCM (8: 1

dx.doi.org/10.1021/ic3023437 | Inorg. Chem. 2013, 52, 464–473

mL) at −10 °C. Crystals suitable for XRD analysis were obtained from the THF-MeCN solution of complex **5** layered with hexane-diethyl ether at −20 °C for 2 weeks and washed with cold THF three times (yield 0.036 g, 13%). IR (cm^{-1}): 1750 (s), 1656 (vs) (ν_{NO}) (KBr). Absorption spectrum (CH_2Cl_2) [λ_{max}, nm (ε, M^{-1} cm^{-1})] (183 K): 375 (1014), 495 (346), 592 (203). Anal. Calcd. for $C_{72}H_{60}P_4FeN_7O_{11}$: C, 62.65; H, 4.42; N, 7.11. Found: C, 62.50; H, 4.58; N, 7.12.

Reaction of $\{Fe(NO)_2\}^9$ DNIC 3 and Bis-(diethylthiocarbamoyl) disulfide $(S_2CNEt_2)_2$. Complex **3** (0.078 g, 0.1 mol) and $(S_2CNEt_2)_2$ (0.0296 g, 0.1 mol) were dissolved in CH_2Cl_2 (4 mL) at −10 °C. The reaction mixture was stirred for 1 h at −10 °C. The reaction was monitored by FT-IR spectroscopy. The IR ν_{NO} stretching frequencies shifting from 1800, 1718 cm^{-1} to 1712 cm^{-1} was assigned to the formation of $\{Fe(NO)\}^7$ $[(NO)Fe(S_2CNEt_2)_2]$.[10] The resulting mixture was stirred for additional 24 h at ambient temperature in the absence of light. The complete shift of IR ν_{NO} stretching frequency from 1712 cm^{-1} to 1847 cm^{-1} indicated the formation of $\{Fe(NO)\}^6$ $[(NO)(\kappa^1\text{-}NO_2)Fe(S_2CNEt_2)_2]$ (**7**).[10a] The resulting mixture was dried under vacuum. The crude product was redissolved in THF and was filtered through Celite to remove the insoluble solid. The filtrate was concentrated to about 2 mL, and hexane (30 mL) was then added slowly to the layer above the brown solution. The flask was tightly sealed and kept in the refrigerator at −20 °C for 3 weeks to yield the brown crystals of complex **7** suitable for XRD analysis. To trap the produced redundant nitrogen dioxide ($\cdot NO_2$), the reaction of complex **3** (0.078 g, 0.1 mol), $(S_2CNEt_2)_2$ (0.0296 g, 0.1 mol), and $\{Fe(NO)\}^7$ $[(NO)Fe(S_2CNEt_2)_2]$ (0.011 g, 0.03 mol) was conducted. The complete shift of IR ν_{NO} stretching frequencies from 1800, 1718, 1712 cm^{-1} (mixture of complex **3** and $[(NO)Fe(S_2CNEt_2)_2]$) to 1847 cm^{-1} indicated the formation of $\{Fe(NO)\}^6$ complex **7** (65% $\cdot NO_2$ was trapped).[10a] The resulting mixture was dried under vacuum. The crude product was redissolved in THF and was filtered through Celite to remove the insoluble solid. Addition of a large amount of hexane into the filtrate led to the precipitation of brown solid complex **7**. IR (cm^{-1}): 1814 (ν_{NO}) (KBr); 1835 (ν_{NO}) (THF); 1847 (ν_{NO}) (CH_2Cl_2).

Reaction of Complex 7 and Dimethyl Sulfide (Me_2S) in the Presence of Imidazole. The THF solution (2 mL) of complex **7** (0.042 g, 0.1 mmol) and imidazole (0.027 g, 0.4 mmol) was prepared under N_2 atmosphere in a vial. The vial containing THF solution of complex **7** and imidazole was then placed in a larger vial containing the THF-MeCN solution of $[PPN]_2[S_5Fe(\mu\text{-}S)_2FeS_5]$ (0.038 g, 0.025 mmol).[9g] The larger vial was then capped with a well-sealed septum. 100-fold of dimethyl sulfide (0.74 mL) was then added into the vial containing THF solution of complex **7** and imidazole by syringe. The mixture solution of complex **7**, imidazole, and Me_2S was stirred for 48 h at room temperature in the absence of light. Then the resulting green solution in the larger vial was transferred to a Schlenk tube and dried under vacuum. The remaining dark green crude solid was redissolved in THF and filtered through Celite to remove insoluble solid. Addition of hexane into the filtrate led to the precipitation of the known dark green solid $[PPN][S_5Fe(NO)_2]$ (70%) characterized by its IR spectrum.[9g] At the same time, the resulting green solution (ν_{NO} 1716 s cm^{-1} (THF)) in the small vial was transferred to a Schlenk tube, and was then filtered through Celite to remove the insoluble solid. Hexane was added into the filtrate to precipitate the insoluble green solid $\{Fe(NO)\}^7$ $[(NO)Fe(S_2CNEt_2)_2]$ (**6**) (yield 0.03 g, 77%).[10] To characterize the produced DMSO, C_4D_8O (2 mL) was used to dissolve complex **7** and imidazole. The C_4D_8O solvent containing DMSO was trapped by liquid nitrogen under vacuum. The trapped DMSO in C_4D_8O was identified by ^1H NMR (δ 2.56 ppm (C_4D_8O)).

EPR Spectroscopy. EPR measurements were performed at X-band using a Bruker ELEXSYS E580 spectrometer equipped with an ELEXSYS super high sensitivity probehead cavity. At 4 K, X-band EPR spectrum of complex **2** (CH_2Cl_2) was obtained with frequency at 9.484 GHz. The microwave power and modulation amplitude are 19.971 mW and 0.8 G at 100.00 kHz, respectively. At 220 K (300 K for **4**), X-band EPR spectra of complexes **3** (CH_2Cl_2) and **4** (THF) were obtained with frequencies at 9.641 and 9.655 GHz, respectively. The microwave power and modulation amplitude are 0.752 mW (15 mW for **4**) and 0.8 G at 100.00 kHz, respectively. At 200 and 77 K, X-band EPR spectra of complex **5** (CH_2Cl_2) under the presence of 50-fold $[PPN][NO_3]$ were obtained with frequencies at 9.394 and 9.482 GHz, respectively. The microwave power and modulation amplitude are 1.997 mW (19.971 mW for 77 K) and 0.8 G at 100.00 kHz, respectively.

Magnetic Measurements. The magnetic data were recorded on a SQUID magnetometer (SQUID-VSM Quantum Design Company) under 1 T external magnetic field in the temperature range 2−300K. The magnetic susceptibility data were corrected with temperature independent paramagnetism (TIP, 2×10^{-4} cm^3 mol^{-1}), and ligands' diamagnetism by the tabulated Pascal's constants.[12] For high-spin ferrous (Fe(II)) center ($S = 2$) of complexes **1-PPN** and **1-Et_4N**, spin Hamiltonian ($\hat{H} = D(\hat{S}_z^2 - 1/3 \times \hat{S}^2) + g\beta\hat{S}H$) was used to describe the negative axial zero field splitting within complexes **1-PPN** and **1-Et_4N**. The best fit to the experimental magnetic data of complex **1-PPN** gives $g = 2.262 \pm 0.001$, $|D| = 5.922 \pm 0.058$ cm^{-1}, and $\theta = -1.156 \pm 0.046$ K with $R^2 = 0.999$. Moreover, the best fit of the experimental magnetic data of complex **1-Et_4N** is $g = 2.110 \pm 0.001$, $|D| = 4.365 \pm 0.162$ cm^{-1}, and $\theta = -4.489 \pm 0.272$ K with $R^2 = 0.997$.

XAS Measurements. All Fe K edge spectra were carried out at NSRRC, Hsinchu, Taiwan, and were recorded at room temperature. Experiments were performed in transmission mode at the BL17C wiggler beamline with a double crystal Si(111) monochromator. The energy resolution $\Delta E/E$ was estimated to be about 2×10^{-4}. High harmonics were rejected by Rh-coated mirrors. The spectra were scanned from 6.912 to 8.006 keV. A reference Fe foil was always measured simultaneously, in which the first inflection point at 7112.0 eV of the Fe foil spectrum was used for energy calibration. Ion chambers used to measure the incident (I_0) and transmitted (I) beam intensities were filled with a mixture of N_2 and He gases and a mixture of N_2 and Ar gases, respectively. The spectra were normalized based on the procedures reported by Solomon and co-workers.[13] A smooth background was removed from all spectra by fitting a straight line to the pre-edge region and then subtracting this straight line from the entire spectrum. Normalization of the data was accomplished by fitting a flat polynomial to the postregion and by normalizing the edge jump to 1.0 at 7400 eV for Fe K-edge spectra.

X-ray Crystallography. Crystallographic data and structure refinements parameters of complexes **1**, **2**, **3**, **4**, and **5** are summarized in the Supporting Information, Tables S1−S5. The crystals of complexes **1**, **2**, **3**, **4**, **5**, and **7** chosen for XRD studies were measured in sizes $0.28 \times 0.25 \times 0.25$ mm^3, $0.25 \times 0.20 \times 0.20$ mm^3, $0.15 \times 0.15 \times 0.12$ mm^3, $0.25 \times 0.10 \times 0.08$ mm^3, $0.22 \times 0.17 \times 0.10$ mm^3, and $0.20 \times 0.17 \times 0.07$ mm^3, respectively. Each crystal was mounted on a glass fiber and quickly coated in epoxy resin. Unit-cell parameters were obtained by least-squares refinement. Diffraction measurements were carried out on a Bruker X8 APEX II CCD diffractometer for complexes **1**, **2**, **3**, **4**, **5**, and **7** with graphite-monochromated Mo K_α radiation ($\lambda = 0.7107$ Å) and between 1.64 and 26.36° for complex **1**, between 1.46 and 26.41 for complex **2**, between 2.11 and 25.09° for complex **3**, between 1.31 and 26.41° for complex **4**, between 1.47 and 26.41° for complex **5**, and between 2.04 and 26.43° for complex **7**. Least-squares refinement of the positional and anisotropic thermal parameters of all non-hydrogen atoms and fixed hydrogen atoms was based on F^2. A semiempirical from equivalent absorption correction was made for **1**, **2**, **3**, **4**, **5**, and **7**.[14] The SHELXTL structure refinement program was employed.[15] For complex **2**, remarkable electron densities located around O13 and O13′ were observed as N7/O13 and N7′/O13′ were assigned to NO. Moreover, the nitrato assignment of N5/O7/O8/O9 and N5′/O7′/O8′/O9′ caused unusual large thermal ellipsoids of O8/O9 and O8′/O9′. This implicated that the same site in two unit cells is occupied by different types of ligands, NO, and monodentate nitrato ligand. The partition ratio 68.5: 31.5 is used to model substitutional disorder.

dx.doi.org/10.1021/ic3023437 | Inorg. Chem. 2013, 52, 464−473

■ ASSOCIATED CONTENT

Supporting Information

X-ray crystallographic files in CIF format for structure determinations of $[PPN]_2[Fe(\kappa^2\text{-}O_2NO)_4]$ (**1-PPN**), $[PPN]_2[(\kappa^2\text{-}O_2NO)(\kappa^1\text{-}O_2NO)_3Fe(NO)]$ (**2**), $[PPN][(\kappa^1\text{-}ONO_2)_2Fe(NO)_2]$ (**3**), $[PPN][(\kappa^1\text{-}ONO_2)(ONO)Fe(NO)_2]$ (**4**), $[PPN]_2[(\kappa^1\text{-}ONO_2)_2(\kappa^2\text{-}O_2NO)Fe(NO)_2]$ (**5**), and $[(NO)(\kappa^1\text{-}NO_2)Fe(S_2CNEt_2)_2]$ (**7**). This material is available free of charge via the Internet at http://pubs.acs.org.

■ AUTHOR INFORMATION

Corresponding Author

*E-mail: wfliaw@mx.nthu.edu.tw (W.-F.L.), fttsai@mx.nthu.edu.tw (F.-T.T.).

Notes

The authors declare no competing financial interest.

■ ACKNOWLEDGMENTS

We gratefully acknowledge financial support from the National Science Council of Taiwan. The authors thank Miss Pei-Lin Chen and Mr. Ting-Shen Kuo for single-crystal X-ray structure determinations. We also thank Dr. Jyh-Fu Lee and National Synchrotron Radiation Research Center of Taiwan (NSRRC) for their support on the hardware and software applied in this work.

■ REFERENCES

(1) (a) Butler, A. R.; Megson, I. L. *Chem. Rev.* **2002**, *102*, 1155−1165. (b) Vanin, A. F. *Nitric Oxide* **2009**, *21*, 1−13. (c) Tonzetich, Z. J.; McQuade, L. E.; Lippard, S. J. *Inorg Chem* **2010**, *49*, 6338−6348. (d) Stamler, J. S.; Singel, D. J.; Loscalzo, J. *Science* **1992**, *258*, 1898−1902. (e) Stamler, J. S. *Cell* **1994**, *78*, 931−936. (f) Ding, H.; Demple, B. *Proc. Natl. Acad. Sci. U.S.A.* **1997**, *94*, 8445−8447.

(2) (a) Foster, M. W.; Cowan, J. A. *J. Am. Chem. Soc.* **1999**, *121*, 4093−4100. (b) Cooper, C. E. *Biochim. Biophys. Acta* **1999**, *1411*, 290−309.

(3) (a) Lundberg, J. O.; Weitzberg, E.; Gladwin, M. T. *Nat. Rev. Drug Discovery* **2008**, *7*, 156−167. (b) Tennyson, A. G.; Lippard, S. J. *Chem. & Biol.* **2011**, 1211−1220. (c) Bryan, N. S.; Fernandez, B. O.; Bauer, S. M.; Garcia-Saura, M. F.; Milsom, A. B.; Rassaf, T.; Maloney, R. E.; Bharti, A.; Rodriguez, J.; Feelish, M. *Nat. Chem. Biol.* **2005**, *1*, 290−297. (d) Gladwin, M. T. *Nat. Chem. Biol.* **2005**, *1*, 245−246. (e) Gladwin, M. T.; Shelhamer, J. H.; Schechter, A. N.; Pease-Fye, M. E.; Waclawiw, M. A.; Panza, J. A.; Ognibene, F. P.; Cannon, R. O., III. *Proc. Natl. Acad. Sci. U.S.A.* **2000**, *97*, 11482−11487.

(4) (a) Nasri, H.; Ellison, M. K.; Shaevitz, B.; Gupta, G. P.; Scheidt, W. R. *Inorg. Chem.* **2006**, *45*, 5284−5290. (b) Wyllie, G. R. A.; Munro, O. Q.; Schulz, C. E.; Scheidt, W. R. *Polyhedron* **2007**, *26*, 4664−4672. (c) Kurtikyan, T. S.; Gulyan, G. M.; Martirosyan, G. G.; Lim, M. D.; Ford, P. C. *J. Am. Chem. Soc.* **2005**, *127*, 6216−6224. (d) Kurtikyan, T. S.; Hovhannisyan, A. A.; Hakobyan, M. E.; Patterson, J. C.; Iretskii, A.; Ford, P. C. *J. Am. Chem. Soc.* **2007**, *129*, 3576−3585. (e) Gulyan, G. M.; Kurtikyan, T. S.; Ford, P. C. *Inorg. Chem.* **2008**, *47*, 787−789. (f) Kurtikyan, T. S.; Martirosyan, G. G.; Hakobyan, M. E.; Ford, P. C. *Chem. Commun.* **2003**, 1706−1707.

(5) (a) Jiang, J.; Holm, R. H. *Inorg. Chem.* **2005**, *44*, 1068−1072. (b) Majumdar, A.; Pal, K.; Sarkar, S. *J. Am. Chem. Soc.* **2006**, *128*, 4196−4197.

(6) (a) Tsai, F.-T.; Kuo, T.-S.; Liaw, W.-F. *J. Am. Chem. Soc.* **2009**, *131*, 3426−3427. (b) Tsai, F.-T.; Chen, P.-L.; Liaw, W.-F. *J. Am. Chem. Soc.* **2010**, *132*, 5290−5299.

(7) (a) Lu, T.-T.; Chiou, S.-J.; Chen, C.-Y.; Liaw, W.-F. *Inorg. Chem.* **2006**, *45*, 8799−8806. (b) Harrop, T. C.; Song, D.; Lippard, S. J. *J. Am. Chem. Soc.* **2006**, *128*, 3528−3529.

(8) (a) Hess, J. L.; Hsieh, C.-H.; Brothers, S. M.; Hall, M. B.; Darensbourg, M. Y. *J. Am. Chem. Soc.* **2011**, *133*, 20426−20434. (b) Hess, J. L.; Hsieh, C.-H.; Reibenspies, J. H.; Darensbourg, M. Y. *Inorg. Chem.* **2011**, *50*, 8541−8552. (c) Hsieh, C.-H.; Darensbourg, M. Y. *J. Am. Chem. Soc.* **2010**, *132*, 14118−14125. (d) Wang, J.-H.; Chen, C.-H. *Inorg. Chem.* **2010**, *49*, 7644−7646. (e) Tonzetich, Z. J.; Do, L. H.; Lippard, S. J. *J. Am. Chem. Soc.* **2009**, *131*, 7964−7965. (f) Wang, R.; Wang, X.; Sundberg, E. B.; Nguyen, P.; Grant, G. P.; Sheth, C.; Zhao, Q.; Herron, S.; Kantardjieff, K. A.; Li, L. *Inorg. Chem.* **2009**, *48*, 9779−9785.

(9) (a) Yeh, S.-W.; Lin, C.-W.; Li, Y.-W.; Hsu, I.-J.; Chen, C.-H.; Jang, L.-Y.; Lee, J.-F.; Liaw, W.-F. *Inorg. Chem.* **2012**, *51*, 4076−4087. (b) Tsou, C.-C.; Liaw, W.-F. *Chem.—Eur. J.* **2011**, *17*, 13358−13366. (c) Lu, T.-T.; Chen, C.-H.; Liaw, W.-F. *Chem.—Eur. J.* **2010**, *16*, 8088−8095. (d) Tsai, M.-C.; Tsai, F.-T.; Lu, T.-T.; Tsai, M.-L.; Wei, Y.-C.; Hsu, I.-J.; Lee, J.-F.; Liaw, W.-F. *Inorg. Chem.* **2009**, *48*, 9579−9591. (e) Shih, W.-C.; Lu, T.-T.; Yang, L.-B.; Tsai, F.-T.; Chiang, M.-H.; Lee, J.-F.; Chiang, Y.-W.; Liaw, W.-F. *J. Inorg. Biochem.* **2012**, *113*, 83−93. (f) Hung, M.-C.; Tsai, M.-C.; Liaw, W.-F. *Inorg. Chem.* **2006**, *45*, 6041−6047. (g) Tsai, M.-L.; Chen, C.-C.; Hsu, I.-J.; Ke, S.-C.; Hsieh, C.-H.; Chiang, K.-A.; Lee, G.-H.; Wang, Y.; Liaw, W.-F. *Inorg. Chem.* **2004**, *43*, 5159−5167.

(10) (a) Ileperuma, O. A.; Feltham, R. D. *Inorg. Chem.* **1977**, *16*, 1876−1883. (b) Ileperuma, O. A.; Feltham, R. D. *J. Am. Chem. Soc.* **1976**, *98*, 6039−6040. (c) Colapietro, M.; Domenicano, A.; Scaramuzza, L.; Vaciago, A.; Zambonelli, L. *Chem. Commun.* **1967**, 583−584. (d) Davies, G. R.; Mais, R. H. B.; Owston, P. G. *Chem. Commun.* **1968**, 81−82. (e) Davies, G. R.; Jarvis, J. A.; Kilbourn, B. K.; Mais, R. H. B.; Owston, P. G. *J. Chem. Soc. A* **1970**, 1275−1283.

(11) (a) Khin, C.; Heinecke, J.; Ford, P. C. *J. Am. Chem. Soc.* **2008**, *130*, 13830−13831. (b) Kurtikyan, T. S.; Hovhannisyan, A. A.; Iretskii, A. V.; Ford, P. C. *Inorg. Chem.* **2009**, *48*, 11236−11241.

(12) (a) Bain, G. A.; Berry, J. F. *J. Chem. Educ.* **2008**, *85*, 532−536. (b) Kahn, O. *Molecular Magnetism*; VCH: New York, 1993.

(13) (a) Glaser, T.; Hedman, B.; Hodgson, K. O.; Solomon, E. I. *Acc. Chem. Res.* **2000**, *33*, 859−868. (b) Solomon, E. I.; Hedman, B.; Hodgson, K. O.; Dey, A.; Szilagyi, R. K. *Coord. Chem. Rev.* **2005**, *249*, 97−129. (c) Rose, K.; Shadle, S. E.; Eidsness, M. K.; Kurtz, D. M., Jr.; Scott, R. A.; Hedman, B.; Hodgson, K. O.; Solomon, E. I. *J. Am. Chem. Soc.* **1998**, *120*, 10743−10747.

(14) (a) North, A. C. T.; Phillips, D. C.; Mathews, F. S. *Acta Crystallogr.* **1968**, *A24*, 351−359.

(15) Sheldrick, G. M. *SHELXTL: A Program for Crystal Structure Determination*; Siemens Analytical X-ray Instruments, Inc.: Madison, WI, 1994.